Available online at www.sciencedirect.com
ScienceDirect
Mendeleev Commun., 2017, **27**, 188–191
Mendeleev Communications

Sorption of Am^{III} onto orthophosphates of the rare-earth elements with different crystal structures

Nadezhda N. Gracheva,[a] Anna Yu. Romanchuk,[a] Ksenia I. Bryukhanova,[b] Konstantin S. Gavrichev[b] and Stepan N. Kalmykov*[a,c]

[a] *Department of Chemistry, M. V. Lomonosov Moscow State University, 119991 Moscow, Russian Federation. Fax: +7 495 939 3220; e-mail: stepan@radio.chem.msu.ru*
[b] *N. S. Kurnakov Institute of General and Inorganic Chemistry, Russian Academy of Sciences, 119991 Moscow, Russian Federation*
[c] *A. N. Frumkin Institute of Physical Chemistry and Electrochemistry, Russian Academy of Sciences, 119071 Moscow, Russian Federation*

DOI: 10.1016/j.mencom.2017.03.028

The effect of ionic strength, pH value, and particles morphology on the Am^{III} sorption onto $LnPO_4$ with different crystalline structures, *i.e.*, monazite, xenotime, and rhabdophane, was established. The sorption capacity of the $LnPO_4$ was found to be independent of its crystal structure and equal to *ca.* 1 μmol m^{-2}.

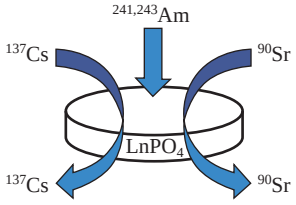

Nowadays, huge amounts of radioactive wastes with different composition are accumulated as the result of civic and military nuclear activities.[1,2] Therefore, the technologies for processing, separation, conditioning, and disposal of radioactive wastes should be developed. The largest amount of the nuclear wastes exists in the liquid form but has to be transferred to the solid state due to the security requirements.

Synthetic phosphate-based materials can be used as the sorbents for accumulation of radionuclides (especially actinides and lanthanides) from liquid nuclear wastes. A number of publications on high sorption capacity of different materials such as $Th_4P_2O_7(PO_4)_4$, ZrP_2O_7, $Zr_2O(PO_4)_2$, $LaPO_4$, and $La(PO_3)_3$ towards U^{VI} is limited.[3–9] Hence, further understanding of sorption processes is still required.

The large-scale production of diverse nanomaterials with well-controlled shape, size, phase purity, crystallinity, and chemical composition is one of the most challenging issues of inorganic synthesis. The possibility of obtaining lanthanide phosphates nanowires, nanobelts, nanotubes, nanorods, and nanoparticles was widely studied for last decades.[10–14] This led to the discovery of the most suitable methods of synthesis: (*a*) precipitation of Ln phosphate salts from the aqueous solutions and (*b*) hydrothermal process. The method *a* makes it possible to prepare spherical particles of the rare-earth elements (REE) phosphates with hexagonal structure.[15–17] Subsequent annealing enables one to obtain monoclinic $LnPO_4$ with spherical microcrystal morphology. The method *b* allows one to control the morphology and chemical composition of the phosphates by varying the initial amount of reagents and reaction conditions (pH, solvent, Ln : P molar ratio, temperature, and reaction time).[18–22]

Lanthanide orthophosphates have several main polymorphic forms, namely hexagonal (rhabdophane),[17,19] tetragonal (xenotime),[19,23] and monoclinic (monazite)[19] modifications. There are two structural types of anhydrous $LnPO_4$. Light REE (La–Gd) form orthophosphates with the monoclinic monazite structure, while heavy REE (Tb–Lu, Y) form the tetragonal xenotime structure. Hydrated hexagonal structure $LnPO_4 \cdot (0.5 + x)H_2O$ is the low-temperature phase of the light lanthanides.[24] At high temperatures (600–900 °C) the hexagonal structure could be transformed into more stable monoclinic one.[15,17] It is important to note the dimorphism exhibited by orthophosphates of transition range REE (Gd–Dy).[25,26]

In this paper, we address orthophosphates of REE ($LnPO_4$) with different crystalline structures as perspective sorbents for minor actinides, particularly Am^{III}. The aim was to determine influence of the most important features of sorption process, in particular ionic strength, pH, particles morphology, crystal structure, and composition of $LnPO_4$, on the rate and value of sorption.

The growth of nanowhiskers (or nanorods) and bulk-particles of REE orthophosphates was carried out by the hydrothermal technique under various conditions[†] using the method described earlier.[27] The limits of the reaction temperature (115–200 °C) were determined by the necessity to create sufficient pressure in the autoclave and by the heat stability of the Teflon liner. Time limits were determined by crystal growth kinetics and instrument characteristics.

[†] High-purity REE oxides La_2O_3, Pr_6O_{11}, Nd_2O_3, Gd_2O_3, Dy_2O_3, Tb_4O_7 (99.99 wt%), ammonium dihydrophosphate $NH_4H_2PO_4$ (analytical grade), hydrochloric acid (pure grade, 34.68 wt%), and distilled water were used as the starting reagents.

Synthesis. The REE oxide dissolved in hydrochloric acid was added to ammonium dihydrophosphate at a La : P molar ratio of 1:1. The pH value of the solution was subsequently adjusted to 0–1 using conc. HCl. The resulting suspension was poured into a steel autoclave with a Teflon liner (filling factor, 75–85%). The autoclave was sealed and maintained at reaction temperature of 115–200 °C for 48–60 h and then slowly (1 K min^{-1}) cooled down to room temperature. The resulting products were separated by filtration, repeatedly washed with distilled water, and finally dried at 80 °C in air.

Only synthesis of bulk $NdPO_4$ particles with monazite structure was performed by direct precipitation at pH ~ 7 upon mixing the solution of $Nd(NO_3)_3$ with the solution of $NH_4H_2PO_4$.

Table 1 The synthesis conditions and characteristics of studied $LnPO_4$ samples.

Type of mineral	Type of unit cell	Composition	Synthesis conditions, T/°C (t/h)	Sample morphology	Surface area / $m^2\ g^{-1}$
Monazite	monoclinic	$LaPO_4$	200 (48)	whisker	12
		$PrPO_4$	160 (55)	whisker	19
		$NdPO_4$	200 (60)	whisker	20
		$NdPO_4$	direct precipitation	bulk	2
Rhabdophane	hexagonal[a]	$LaPO_4{\cdot}0.44\,H_2O$	115 (60)	nanowhisker/ nanorod	38
	hexagonal	$GdPO_4{\cdot}0.46\,H_2O$	180 (48)	bulk	10
Xenotime	tetragonal	$DyPO_4$	180 (55)	nanoparticle	19
		$TbPO_4$	160 (55)	nanoparticle	16

[a] Hexagonal form + impurity 1–2% of monoclinic form.

The main characteristics of lanthanide orthophosphates samples obtained under different hydrothermal conditions are given in Table 1.

The XRD patterns‡ of the obtained lanthanide orthophosphates are shown in Figure S1 (see Online Supplementary Materials). All reflections can be readily indexed to monoclinic phase (space group $P2_1/n$) for $LnPO_4{\cdot}xH_2O$ (Ln = La, Pr, Nd), hexagonal phase (space group $P3_121$) for $LnPO_4{\cdot}xH_2O$ (Ln = La, Gd), and tetragonal phase (space group $I4_1/amd$) for $LnPO_4$ (Ln = Tb, Dy). The monoclinic phase peaks (1–2%) were also detected in diffractograms of the $LaPO_4{\cdot}xH_2O$ sample. The intensity and shape of the diffraction peaks suggest that the samples were crystalline and without contribution of amorphous phase. The unit cell parameters of lanthanide orthophosphates powders, calculated from XRD patterns, are consistent with those reported in the JCPDS PDF2 cards and literature.

The SEM images‡ of the samples are illustrated in Figures 1 and S2. Figure 1(*a*),(*b*) exhibits the SEM images of monoclinic $LaPO_4$ whiskers (diameter d from 40 to 50 nm and length l from 400 to 900 nm) and $NdPO_4$ bulk particles, respectively.

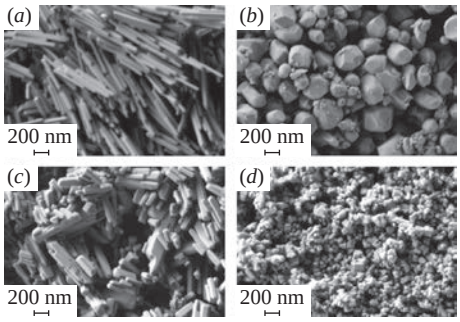

Figure 1 SEM images of the obtained by hydrothermal treatment (*a*) monazite-type $LaPO_4$, (*b*) monazite-type $NdPO_4$ bulk particles, (*c*) rhabdophane-type $GdPO_4{\cdot}0.46H_2O$, and (*d*) xenotime-type $TbPO_4$.

‡ *Samples characterization*. The crystal phase and purity of the obtained samples were characterized by X-ray powder diffraction (XRD) using SHIMADZU XRD-600 diffractometer with CuKα radiation (a = 1.5418 Å, graphite monochromator, reflection geometry). The calculated cell lattice constant of the products were consistent with the standard JCPDS data. The size and morphology of particles were studied by the scanning electron microscopy (SEM) using CrossBeam Zeiss NVision 40 (U = 1 kV). The thermal behavior and the composition of the samples were investigated simultaneously by differential scanning calorimetry and thermogravimetric analysis (DSC/TG) using a Netzsch STA 449F1 Jupiter® apparatus in the inert gas (helium 6.0) flow. The specific surface area of powder was determined by BET technique (ASAP 2010N, Micrometrics).

Figure 1(*c*),(*d*) shows the SEM images of hexagonal nanorods/nanowhiskers $GdPO_4{\cdot}xH_2O$ bulks (with $d \approx 50$–180 nm, $l \approx$ ≈ 200 nm–1 μm) and the tetragonal $TbPO_4$ nanoparticles with the diameter of ~50 nm. The high degree of samples crystallinity is in good agreement with the results of XRD.

The samples were studied by DSC/TG analysis‡ to determine the amount of residual water in the specimens. From the TG curve the absence of water molecules in the $LnPO_4$ (Ln = La, Pr, Nd, Tb, Dy) samples was established. On the contrary, TGA measurements and stoichiometry calculations showed that the studied hexagonal modifications of La and Gd orthophosphates contain 0.44 and 0.46 mol of H_2O, respectively. These specimens of hexagonal modifications are stable up to 850 °C (Figures S3–S5).

Three $LnPO_4$ samples with different crystal structures (monazite, xenotime, rhabdophane) were examined as potential scavengers for Am^{III}.§ The kinetics of Am^{III} sorption was studied at 5×10^{-10} M radionuclide concentration. To estimate the difference in free surface area, the solid phase concentration of 1.65 $m^2\ dm^{-3}$ was used. The steady state conditions for $LnPO_4$ samples with different structures were reached within 10 min [Figure 2(*a*)]. This fact

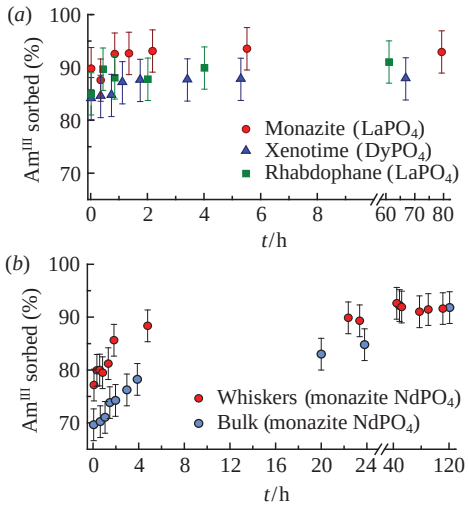

Figure 2 The kinetics of Am^{III} sorption onto $LnPO_4$ samples (*a*) with different crystal structures (pH 4, $[Am^{III}] = 5\times10^{-10}$ M, $[LnPO_4] = 1.65\ m^2\ dm^{-3}$) and (*b*) different particles morphology (pH 4, $[Am^{III}] = 5\times10^{-9}$ M, $[NdPO_4] =$ $= 0.84\ m^2\ dm^{-3}$, I = 0.01 M $NaClO_4$).

§ *Sorption experiments*. The sorption of Am^{III} onto the $LnPO_4$ samples was investigated using two americium isotopes (^{241}Am and ^{243}Am). Their radiochemical purity was confirmed by γ- and α-spectrometric techniques. The sorption experiments were performed in plastic vials. It was found that under the experimental conditions the Am^{III} sorption onto the vial walls was negligible. The $LnPO_4$ suspension was prepared in $NaClO_4$ (analytical grade) solution as the background electrolyte and was preconditioned for several days. $NaClO_4$ was chosen because of its very low complexation ability. After addition of aliquot of solution containing americium, the pH was adjusted to the desired value by the addition of a small amount of diluted $HClO_4$ or NaOH solution. In the course of the sorption experiment the pH was periodically controlled and adjusted if required. The solid phase was separated by centrifugation at 14000*g* for 20 min (Eppendorf Centrifuge 5418). The sorption was calculated from the difference between the initial Am^{III} radioactivity and that measured after the equilibration. The radioactivity of ^{241}Am or ^{243}Am in solution was determined by the liquid scintillation counting (TriCarb 2700TR, Packard Instruments). Each sample was measured periodically until the constant sorption value was reached.

The mixture of stable europium isotopes and ^{152}Eu isotope was used to obtain sorption isotherm. The experiment was performed as described above. In this sorption experiment the pH was periodically controlled and adjusted to the value of 4.00±0.05. The ^{152}Eu radioactivity was also determined by the liquid scintillation counting.

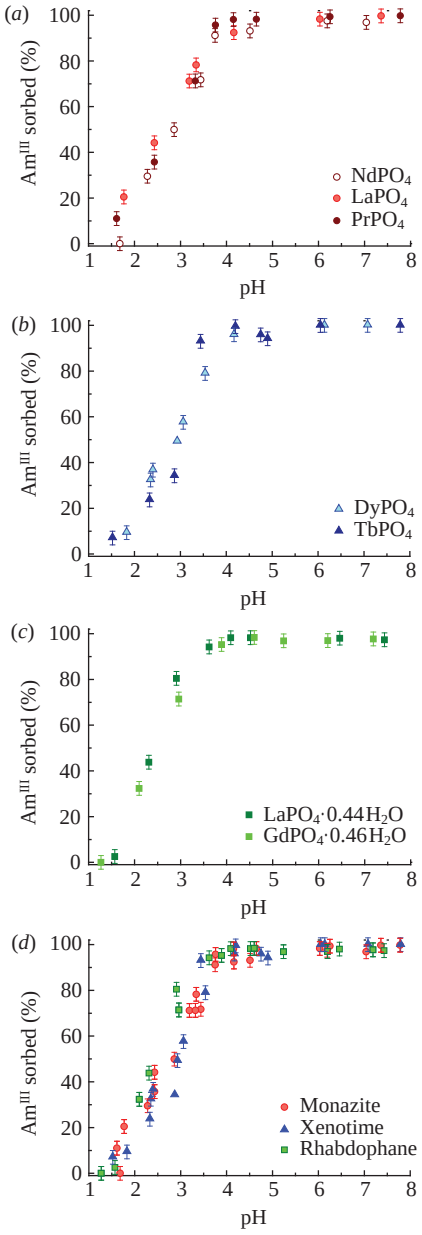

Figure 3 The pH-dependences of Am^{III} sorption onto orthophosphates with (*a*) monoclinic, (*b*) tetragonal, (*c*) hexagonal structure with different cations of REE in the composition; (*d*) summary of all Am^{III} sorption data for different $LnPO_4$ crystal structures ($[Am^{III}] = 5\times10^{-10}$ M, $[LnPO_4] = 0.44$ g dm^{-3}, I = 0.01 M $NaClO_4$).

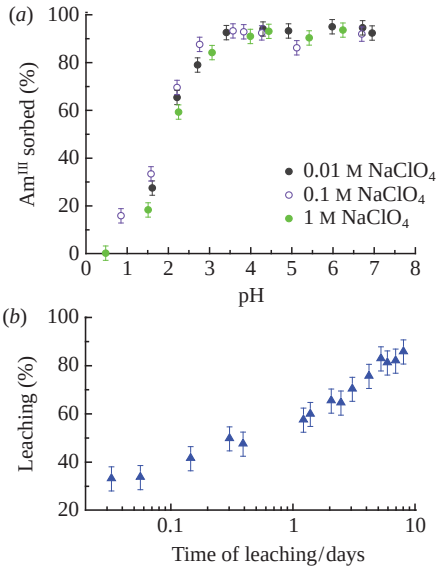

Figure 4 (*a*) The pH-dependences of the Am^{III} sorption by monazite-type $NdPO_4$ from solution with different ionic strength ($[Am^{III}] = 5\times10^{-10}$ M, $[LnPO_4] = 0.44$ g dm^{-3}). (*b*) The kinetics of Am^{III} leaching from the $DyPO_4$ (xenotime) at pH 1.7.

indicates no significant influence of the crystal structure on the Am^{III} sorption at least at the trace-level concentrations.

At lower solid/liquid ratio the sorption of Am^{III} was slightly slower [Figure 2(*b*)]. The sorption of Am^{III} onto large bulk particles ($NdPO_4$) occurred significantly slower than that onto whiskers surface. Pseudo-first-order kinetics equation was used to describe the experimental data. Rate constant was 1×10^{-7} s^{-1} in the case of bulk particles and 6×10^{-7} s^{-1} in the case of whiskers. This difference can be explained by higher reactivity of nanoparticles.

The Am^{III} sorption onto the $LnPO_4$ samples was investigated as a function of pH varying the REE cation in the phosphate (Figure 3). Regardless of the selected cation, the pH-dependences of sorption were the same for the same structure. Thus, there was no influence of the cation of the REE for the same phosphate crystalline structure on the sorption properties of $LnPO_4$ obviously due to the close chemical properties of the lanthanides. The dependences of Am^{III} adsorption on the surface of $LnPO_4$ with different structures were similar [Figure 3(*d*)].

To elucidate the mechanism of Am^{III} sorption, the effect of ionic strength was studied. Figure 4(*a*) shows pH-dependence of Am^{III} sorption onto monazite-type $NdPO_4$ in 0.01, 0.1, and 1 M $NaClO_4$. It was found that changes in ionic strength did not affect Am^{III} sorption. This indicates that Am^{III} forms inner-sphere complexes upon sorption by $LnPO_4$.[28] To determine the reversibility of Am^{III} sorption, the acid leaching at pH 1.7 was performed.¶ Figure 4(*b*) shows typical leaching curve. The kinetics of Am^{III} leaching from the $LnPO_4$ samples is relatively slow as compared to the kinetics of the sorption (Figure 2). However, these data proved the reversibility of Am^{III} sorption.

To determine the sorption capacities for the $LnPO_4$ samples with different crystalline structures, the Eu^{III} sorption isotherms at pH 4.00 (±0.05) were obtained. The Eu^{III} was used as a chemical analogue of Am^{III} in order to make higher sorbate concentrations. In this experiment, the concentration of $LnPO_4$ samples was kept constant, while the concentration of Eu^{III} was varied from 10^{-8} to 10^{-3} M (Figure 5). The isotherms of Eu^{III} sorption onto $LnPO_4$ with different crystal structures were similar. When sorption was expressed in mol g^{-1} units, the sorption isotherm for $LaPO_4{\cdot}xH_2O$ with the rhabdophane structure demonstrated slightly higher sorption than that for other samples [Figure 5(*a*)]. However, when sorption was expressed in mol m^{-2} units, all sorption isotherms coincided [Figure 5(*b*)]. The orthophosphate with hexagonal structure had the largest free surface area (38 m^2 g^{-1}) that explains the higher sorption onto this sample.

All isotherms reached saturation plateau, therefore, the experimental data were fitted using the Langmuir equation:

$$[Eu]_{surface} = Q_{max} K_{La} [Eu]_{solution} / (1 + K_{La} [Eu]_{solution}),$$

where $[Eu]_{surface}$ is the equilibrium concentration of Eu^{III} absorbed onto $LnPO_4$, $[Eu]_{solution}$ is the equilibrium concentration of Eu^{III} in the solution, Q_{max} is the sorption capacity, and K_{La} is Langmuir constant. The calculated Q_{max} values (Table 2) for $LnPO_4$ with different crystal structures were similar (*ca.* 1 μmol m^{-2}).

¶ *Leaching experiments*. Leaching tests were performed for samples with high amount of Am^{III} (>98%) absorbed, usually for samples with pH > 5. The sorption values of these samples were measured first and then the pH was lowered to 1.7 by the addition of conc. $HClO_4$ without changing electrolyte solution. The pH value of 1.7 was chosen because of the low sorption of Am^{III} (<10%) and relatively low solubility of $LnPO_4$ under these conditions. After various time intervals, aliquots of the suspension were collected for measuring Am^{III} concentration in the solution.

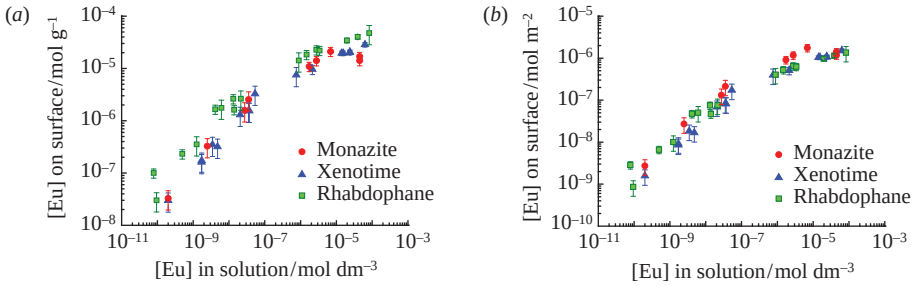

Figure 5 The isotherms of Eu^{III} sorption onto the $LnPO_4$ samples with the different crystal structures. The sorption expressed in (*a*) mol g^{-1} and (*b*) mol m^{-2} units ([$LnPO_4$] = 0.3 g dm^{-3}, pH 4.00 (±0.05), I = 0.01 M $NaClO_4$).

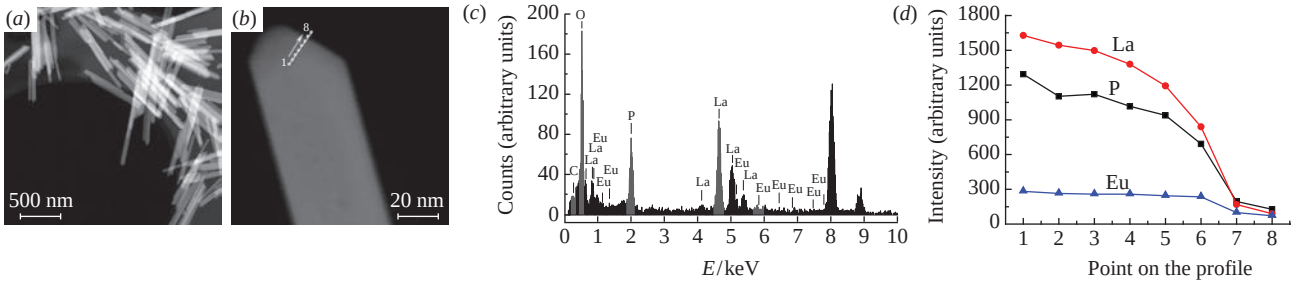

Figure 6 HRTEM examination of the sample of Eu^{III} adsorbed onto $LaPO_4$ whiskers: (*a*),(*b*) TEM images, (*c*) EDX spectrum, (*d*) La, Eu, and P intensity along the profile marked in Figure 6(*b*).

Table 2 Calculated Q_{max} values for $LnPO_4$ samples with different crystal structures.

Structure	Sample	Free surface area/m^2 g^{-1}	R^2	Q_{max}/ μmol g^{-1}	Q_{max}/ μmol m^{-2}
Monazite	$LaPO_4$	12	93	17±2	1.4±0.1
Xenotime	$DyPO_4$	19	97	25±2	1.3±0.1
Rhabdophane	$LaPO_4 \cdot 0.44 H_2O$	38	98	44±2	1.1±0.1

The $LaPO_4$ sample with monoclinic structure was characterized by HRTEM (Figure 6) after contact with Eu^{III}. No formation of any new phases was observed. Shape and morphology of $LnPO_4$ did not change. EDS profile of the Eu distribution showed that europium evenly covered whiskers surface.

In conclusion, the sorption of Am^{III} onto the $LnPO_4$ nanoscale samples with different crystal structures (hexagonal, tetragonal and monoclinic) has been studied. The REE orthophosphates have demonstrated fast kinetics and high sorption capacity towards americium. During sorption process the formation of inner-sphere complexes of Am^{III} has been observed. No significant difference between sorption properties of the $LnPO_4$ samples with different crystal structures and different rare-earth cations has been found. At the same time, the morphology of orthophosphate particles influences the kinetics of Am^{III} sorption.

Radionuclides sorption experiments were supported by the Russian Science Foundation (project no. 14-13-01279). We also acknowledge the 'Nanochemistry and Nanomaterials' user facility at the Department of Chemistry of the M. V. Lomonosov Moscow State University for providing the HRTEM measurements.

Online Supplementary Materials

Supplementary data associated with this article can be found in the online version at doi:10.1016/j.mencom.2017.03.028.

References

1 B. F. Myasoedov and S. N. Kalmykov, *Mendeleev Commun.*, 2015, **25**, 319.
2 M. Yu. Alyapyshev, V. A. Babain and Yu. A. Ustynyuk, *Russ. Chem. Rev.*, 2016, **85**, 943.
3 R. Drot and E. Simoni, *Langmuir*, 1999, **15**, 4820.
4 E. Ordoñez-Regil, R. Drot, E. Simoni and J. J. Ehrhardt, *Langmuir*, 2002, **18**, 7977.
5 R. Drot, C. Lindecker, B. Fourest and E. Simoni, *New J. Chem.*, 1998, **22**, 1105.
6 L. Qian, P. Hu, Z. Jiang, Y. Geng and W. Wu, *Sci. China Chem.*, 2010, **53**, 1429.
7 M. G. Almazan-Torres, R. Drot, F. Mercier-Bion, H. Catalette, C. Den Auwer and E. Simoni, *J. Colloid Interface Sci.*, 2008, **323**, 42.
8 R. Drot, E. Simoni, M. Alnot and J. J. Ehrhardt, *J. Colloid Interface Sci.*, 1998, **205**, 410.
9 E. Ordoñez-Regil, R. Drot and E. Simoni, *J. Colloid Interface Sci.*, 2003, **263**, 391.
10 L. A. Boatner, *Rev. Mineral. Geochem.*, 2002, **48**, 87.
11 H. Meyssamy, K. Riwotzki, A. Kornowski, S. Naused and M. Haase, *Adv. Mater.*, 1999, **11**, 840.
12 H. Onoda, H. Nariai, A. Moriwaki, H. Maki and I. Motooka, *J. Mater. Chem.*, 2002, **12**, 1754.
13 C. Yu, M. Yu, C. Li, X. Liu, J. Yang, P. Yang and J. Lin, *J. Solid State Chem.*, 2009, **182**, 339.
14 Y.-W. Zhang, Z.-G. Yan, L.-P. You, R. Si and C.-H. Yan, *Eur. J. Inorg. Chem.*, 2003, 4099.
15 R. Kijkowska, *J. Mater. Sci.*, 2003, **38**, 229.
16 E. E. Boakye, P. Mogilevsky and R. S Hay, *J. Am. Ceram. Soc.*, 2005, **88**, 2740.
17 K. S. Gavrichev, M. A. Ryumin, A.V. Tyurin, A.V. Khoroshilov, L. P. Mezentseva, A. V. Osipov, V. L. Ugolkov and V. V. Gusarov, *J. Therm. Anal. Calorim.*, 2010, **102**, 809.
18 H. Dong, Y. Liu, P. Yang, W. Wang and J. Lin, *Solid State Sci.*, 2010, **12**, 1652.
19 Y.-P. Fang, A.-W. Xu, R-.Q. Song, H.-X. Zhang, L-.P. You, J.-C. Yu and H.-Q. Liu, *J. Am. Chem. Soc.*, 2003, **125**, 16025.
20 H. Guan and Y. Zhang, *J. Solid State Chem.*, 2004, **177**, 781.
21 J. Ma and Q. Wu, *J. Appl. Crystallogr.*, 2010, **43**, 990.
22 Z.-G.Yan, Y.-W. Zhang, L.-P. You, R. Si and C.-H. Yan, *J. Cryst. Growth*, 2004, **262**, 408.
23 R. Kijkowska, *Thermochim. Acta*, 2003, **404**, 81.
24 R. C. L. Mooney, *Acta Crystallogr.*, 1950, **3**, 337.
25 Y. Hikichi, T. Sasaki, S. Suzuki and K. Murayama, *J. Am. Ceram. Soc.*, 1988, **71**, 354.
26 A. S. Celebi and J. W. Kolis, *J. Am. Ceram. Soc.*, 2002, **85**, 253.
27 K. I. Bryukhanova, G. E. Nikiforova and K. S. Gavrichev, *Nanosystems: Phys. Chem. Math.*, 2016, **7**, 451.
28 S. Goldberg, L. J. Criscenti, D. R. Turner, J. A. Davis and K. J. Cantrell, *Vadose Zone J.*, 2007, **6**, 407.

Received: 7th July 2016; Com. 16/4990